Supporting Information

Ferroelectric Polarization-Enhanced Photoelectrochemical Water Splitting in TiO_2-$BaTiO_3$ Core-Shell Nanowire Photoanodes

Weiguang Yang,[1,2,†] Yanhao Yu,[1,†] Matthew B. Starr,[1]Xin Yin,[1] Zhaodong Li,[1] Alexander Kvit,[3] Shifa Wang,[4] Ping Zhao,[4] Xudong Wang[1,*]

1. Materials Science and Engineering, University of Wisconsin-Madison, Madison WI, 53706, USA

2. Department of Electronic Information Materials, School of Materials Science and Engineering, Shanghai University, Shanghai 200444, China

3. Materials Science Center, University of Wisconsin-Madison, Madison WI, 53706, USA

4. Mechanical and Industrial Engineering, University of Minnesota Duluth, Duluth, MN, 55812, USA

*Email: xudong@engr.wisc.edu

Experimental details:

Hydrothermal growth of TiO_2 nanowire (NW). Rutile TiO_2 NWs were grown on FTO coated glasses via a hydrothermal process. FTO glass was first ultrasonically cleaned in deionized water, acetone and isopropoxide.[1] A dense TiO_2 seed layer was then deposited on FTO surface by spin-coating the seed solution (5000 RPM for 30s) and annealing the substrate at 500 °C for 1h in air. The seed solution contains 20 μL

of 37% HCl, 0.7 mL of titanium (IV) tetraisopropoxide (TTIP), and 10 mL ethanol. Subsequently, the substrate was loaded into a sealed Teflon-lined stainless steel autoclave (50 ml) and reacted in the 170 °C oven for 3.5 h. The reactor was filled with 10 mL of 37% HCl, 10 mL of deionized water and 0.17 mL of TTIP. After cooling down to room temperature, the substrate was rinsed with deionized water and dried in air. Before barium titanate (BTO) conversion or PEC measurement, the TiO_2 NW was annealed at 500 ^oC for 1h in air to remove the organic residues.

Synthesis of the TiO_2/BTO core/shell NWs. TiO_2/BTO core/shell NWs were fabricated by locally converting rutile TiO_2 NWs surface via a hydrothermal reaction. Specifically, the TiO_2 NWs were first immersed in a sealed Teflon-lined stainless steel autoclave (50 ml) that filled with a solution of 0.75 mmol $Ba(OH)_2 \cdot 8H_2O$ in 5 mL diethylene glycol (DEG), 5 mL ethanol, 1.5 mL 2-propanol, 0.6 g tetrabutylammonium hydroxide solution (TBAH, 40 wt%), and 7 mL deionized water. The container was then transferred to oven and reacted at 150-210 ^oC for 2 h. The thickness of BTO shells were controlled by the reaction temperature. After cooling down to room temperature, samples were washed with deionized water, ethanol, and dried in air.

Photoelectrochemical (PEC) measurement. The PEC measurements were carried out using a typical three-electrode electrochemical cell with the TiO_2/BTO core/shell NWs as the working electrode, Pt wire as the counter electrode and a saturated calomel electrode (SCE) as the reference electrode. Three kinds of electrolytes were used including 1M NaOH solution, phosphate buffer solution (pH=7), and phosphate

buffer solution with 1 M Na_2SO_3. During the *J-V* and *V-t* scanning, working electrodes were illuminated by a 150 W Xenon lamp coupled with an AM 1.5 global filter with a light intensity of 100 mW/cm^2. *J-V* and *V-t* curves were recorded using an Autolab PGSTAT302N station. For the poling experiments, before the PEC test, the 150 ^oC TiO_2/BTO NWs was poled by +3 V or -2 V for 5 min in 2 M KCl aqueous solution using Pt wire as counter electrode. The four edges of the substrate and the metal contact region were covered with insulating epoxy resin. 210 ^oC TiO_2/BTO NWs was poled by ±100 V for 20 min using FTO glass as counter electrode in air.

Characterization. SEM observations were performed on Zeiss LEO 1530 field-emission microscopes and TEM measurements were conducted on FEI TF30 microscopes. X-ray diffraction patterns were acquired from the Bruker D8 Discovery with Cu Kα radiation. XPS was done on Thermo Scientific K-alpha XPS instrument. STEM images and EELS spectrum images were acquired on FEI Titan microscope with a CEOS probe aberration-corrector. The absorption spectra were recorded using an Evolution 220 UV-vis spectrophotometer with integrated sphere (ISA 220). Dynamic contact-electrostatic force microscopy (DC-EFM) measurements were carried out by an atomic force microscope (AFM, XE-70, Park system) with a dc voltage of 0 V and an ac modulating voltage having the frequency and amplitude of 18 kHz and 2.5 V, respectively. A modified Sawyer-Tower circuit was adopted to acquire the polarization P vs electric field E loop. A triangular voltage wave V (-1V to +1V, 0.2 Hz) generated from a function generator (Wavetek 29) was applied to the electrodes of the sample. The electric field E was calculated by dividing the applied

voltage V) by the sample thickness d (E=V/d). The resulting charge Q stored on the sample was determined by means of a larger reference capacitor C (10 uF) placed in series with the sample. An electrometer (Keithley 6514) was used to measure the voltage V_c across the capacitor. By multiplying this voltage V_c with the value of the capacitor C, the charge Q across the sample was obtained ($Q=CV_c$). The polarization density was then given by dividing the charge Q by the electrode area A of the sample (P=Q/A).

Calculation details:

From electrostatics, the Poisson equation describes how the charge density at location x ($\rho(x)$) is influenced by the potential at location x ($V(x)$):

$$\frac{d^2V(x)}{dx^2} = \frac{-\rho(x)}{\epsilon_0\epsilon_r} \quad \text{(S1)}$$

Where ϵ_0 and ϵ_r are the electrical permittivity of vacuum and the medium inhabited by the charge, respectively. $V(x)$ can be solved for all x by twice integrating $\rho(x)$, but we first must get ρ as a function of $V(x)$.

In the TiO2 semiconductor, the charge density is comprised of mobile electrons and holes as well as the immobile charged atoms that we attribute to dopant atoms:

$$\rho_{TiO2}(x) = (z_n)(n(x)) + (z_p)(p(x)) + z_d Nd_{TiO2} \quad \text{(S2)}$$

Where z_n, z_p and z_d are the charge of an electron (-1), hole (1) and dopant atom (1) in TiO2, respectively, and $n(x)$, $p(x)$ and Nd_{TiO2} are the charge density of electrons, holes, and dopant atoms, respectively.

The charge density of electrons and holes varies with position because the electrical potential (relative to bulk potential in TiO2) varies as x approaches the heterojunction.

In both semiconductors and solutions, the ratio of concentration of charged species i in bulk (n_i^0) at bulk potential ($\varphi^0 = 0$) to its concentration (n_i) found at any other potential (φ) is taken to depend upon the Boltzmann factor in the following way:

$$n_i = n_i^0 e^{\left(\frac{-z_i e\phi(x)}{kT}\right)} \quad \text{(S3)}$$

where z_i is the charge of ion *i*, and *e* is the charge of the electron, φ is the potential relative to bulk solution, *x* is a measure of distance into solution and perpendicular to

the monolayer surface, *k* is the Boltzmann constant, and *T* is temperature in Kelvin.

Combining equation S2 and S3 results in the following expression for charge density in the semiconductor:

$$\rho_{TiO2}(x) = (z_n)(n_b)e^{\frac{(z_n)V(x)e}{kT}} + (z_p)(p_b)e^{\frac{(z_p)V(x)e}{kT}} + z_d Nd_{TiO2} \quad \text{(S4)}$$

Where n_b and p_b are the bulk concentrations of electrons and holes, respectively.
Applying this same treatment to the liquid solution medium, where H^+ , OH^- and Na^+ ions comprise the charge density, yields the following expression for the charge density in the aqueous medium:

$$\rho_{H_2O}(x) = (z_{H^+})({H^+}_b)e^{\frac{(z_{H^+})V(x)e}{kT}} + (z_{OH^-})({OH^-}_b)e^{\frac{(z_{OH^-})V(x)e}{kT}} + (z_{Na^+})({Na^+}_b)e^{\frac{(z_{Na^+})V(x)e}{kT}} \quad \text{(S5)}$$

Where z_{H^+}, z_{OH^-} and z_{Na^+} are the charge of hydronium (1), hydroxyl (-1) and sodium (1) ions, respectively, and ${H^+}_b$, ${OH^-}_b$ and ${Na^+}_b$ are the bulk concentrations of hydronium, hydroxyl and sodium ions in solution, respectively.
Equations S4 and S5 can be combined with Eq. S1 to yield the following expressions that describe how potential and charge density are interrelated in both the H_2O and TiO_2:

$$\text{In the Semiconductor:} \quad \frac{d^2V}{dx^2} = \frac{-((z_n)(n_b)e^{\frac{(z_n)V(x)e}{kT}} + (z_p)({p_b})e^{\frac{(z_p)V(x)e}{kT}} + z_d Nd_{TiO2})}{\epsilon_0 \epsilon_r} \quad \text{(S6)}$$

$$\text{In the Solution:} \quad \frac{d^2V}{dx^2} = \frac{-((z_{H^+})({H^+}_b)e^{\frac{(z_{H^+})V(x)e}{kT}} + (z_{OH^-})({OH^-}_b)e^{\frac{(z_{OH^-})V(x)e}{kT}} + (z_{Na^+})({Na^+}_b)e^{\frac{(z_{Na^+})V(x)e}{kT}})}{\epsilon_0 \epsilon_r} \quad \text{(S7)}$$

To solve these second order differential equations requires two boundary conditions for each expression.
In the semiconductor, the boundary conditions are as follows:

1. The electric field ($\frac{dV}{dx}$) in the bulk of the TiO_2 is zero.

$$\left(\frac{dV}{dx}\right)_{x=-\infty} = 0 \quad \text{(S8)}$$

2. The electrical potential in the bulk is equal to the Fermi level of TiO_2 ($V_{EF_{TiO2}}$)

$$V_{x=-\infty} = V_{EF_{TiO2}} \quad \text{(S9)}$$

In the solution phase, the boundary conditions are similar:

1. The electric field ($\frac{dV}{dx}$) in the bulk of H_2O is zero.

$$\left(\frac{dV}{dx}\right)_{x=\infty} = 0 \tag{S10}$$

2. The electrical potential in the bulk is equal to the Fermi level of H_2O ($V_{EF_{H2O}}$).

$$V_{x=\infty} = V_{EF_{H2O}} \tag{S11}$$

Applying boundary conditions S8 and S9 to expression S6 during integration yields the following expression for the potential gradient in the TiO2:

$$\frac{dV_{TiO2}}{dx} = \sqrt{-\frac{2kT}{\epsilon_0 \epsilon_{TiO2}}\left[\left(n_b\left(\left[e^{\frac{z_n Ve}{kT}}\right]-1\right)\right)+\left(p_b\left(\left[e^{\frac{z_p Ve}{kT}}\right]-1\right)\right)+\frac{z_{Nd} Nd_{TiO2} Ve}{kT}\right]} \tag{S12}$$

Applying boundary conditions S10 and S11 to expression S7 during integration yields the following expression for the potential gradient in the H_2O:

$$\frac{dV_{H2O}}{dx} =$$

$$\sqrt{-\frac{2kT}{\epsilon_0 \epsilon_{H2O}}\left[\left(({H^+}_b)\left(\left[e^{\frac{(z_{H^+})Ve}{kT}}\right]-1\right)\right)+\left(({OH^-}_b)\left(\left[e^{\frac{(z_{OH^-})Ve}{kT}}\right]-1\right)\right)+\left(({Na^+}_b)\left(\left[e^{\frac{(z_{Na^+})Ve}{kT}}\right]-1\right)\right)\right]} \tag{S13}$$

Up to this point, the derivation of the potential profile in the ZnO (Eq. S12) and H_2O (Eq. S13) have remained independent from one another. To join the two expressions, we make use of two conditions: 1) the potential profile is continuous, and 2) charge is conserved.

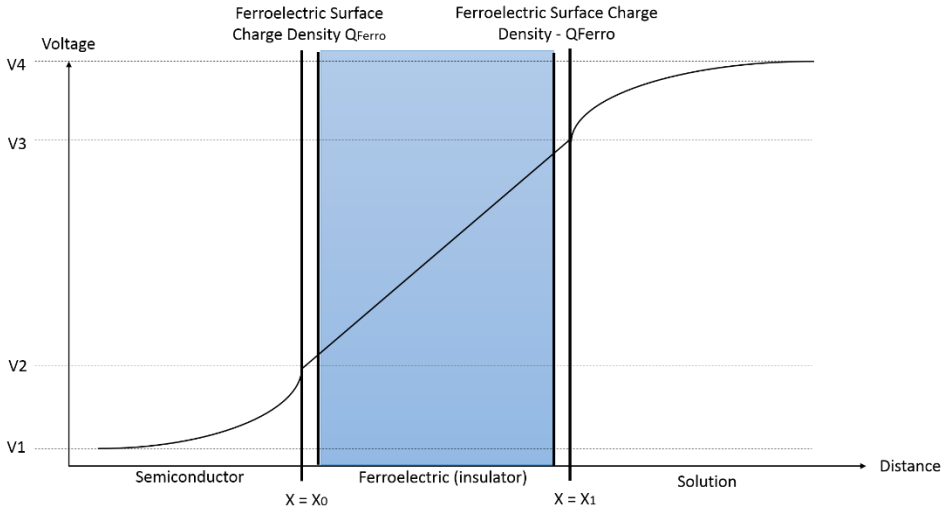

Figure C1: Electrical potential profile through a typical semiconductor/insulator/solution junction.

The electrical potential profile through a typical semiconductor/insulator/solution junction (Fig. C1) is nonlinear in the semiconductor and solution within the vicinity of

the interfaces because the charge density within these regions are non-uniform. There are no free charges inside the insulator and thus the electric field is constant, resulting in a linear potential profile.

At a heterojunction under no external bias, the net charge density ($\frac{C}{m^2}$) in the semiconductor (equivalent to surface charge density Q_{TiO2}) is equal and opposite to the charge density ($\frac{C}{m^2}$) in the solution (equivalent to surface charge density Q_{H2O}). Because the charge densities are equal at the interface, the electric field ($\frac{dV}{dx}$) at the semiconductor and solution interface must be equal:

$$\left(\frac{dV_{TiO2}}{dx}\right)_{x=X_0} = \left(\frac{dV_{H2O}}{dx}\right)_{x=X_1} \quad \text{(S14)}$$

This expression stitches together the physical processes described by expression S12 and S13.

In order to combine the potential profiles generated for the semiconductor (S12) and solution (S13), generated by solving S14, into a cohesive diagram, it is necessary to account for the electrical potential gradient within the insulating layer.

The potential shift across an insulator (V2-V3) is equal to the electric field within the insulator (a constant) multiplied by the distance over which the electric field travels (the insulator thickness: X1-X0):

$$Votlage\ drop\ in\ the\ Insulator = V2 - V3 = \frac{Q_{H2O}(\mathrm{X1-X0})}{\epsilon_0 \epsilon_{Insulator}} = \frac{-Q_{TiO2}(\mathrm{X1-X0})}{\epsilon_0 \epsilon_{Insulator}} \quad \text{(S13)}$$

where $\epsilon_{Insulator}$ is the relative permittivity of the insulating layer. ***When a ferroelectric materials is used for the insulating layer, a remnant electrical polarization within the ferroelectric will alter the electric field present within the insulating layer, deviating the voltage drop from the expression S13.*** The remnant polarization contributes equal and opposite surface charge densities (Q_{Ferro}) to both surfaces:

$$Votlage\ drop\ in\ the\ Insulator = V2 - V3 = \frac{(Q_{H2O}+Q_{Ferro})(\mathrm{X1-X0})}{\epsilon_0 \epsilon_{Insulator}} = \frac{-(Q_{TiO2}-Q_{Ferro})(\mathrm{X1-X0})}{\epsilon_0 \epsilon_{Insulator}} \quad \text{(S14)}$$

Depending on the sign of the charges in the semiconductor and solution medium, and direction of the remnant polarization within the ferroelectric insulator, Q_{Ferro} may act to increase or decrease the field within the insulator caused by Q_{TiO2} and Q_{H2O} (e.g. Fig 5a and 5b).

Checking for physically reasonable values

At every step of the calculation, the properties of the physical environment were checked to ensure that physically reasonable quantities were being produced. A particularly concerning value is the density of charged species in solution at the

insulator/solution interface, care needs to be taken to ensure this density does not exceed atomic density of a condensed phase.

To calculate the maximum charge densities we could physically expect from our model, we modeled the hydrated ions (Na^+, H^+, and OH^-) as hard spheres and fit them into the maximum packing density possible, the close packing structure. Taking OH^- ions as an example, each with a hydration diameter (d) of 3.5 Å, the maximum 3D packing density possible is given by:

$$\text{Maximum 3D Density} = \frac{Tota \quad \text{ions}}{\text{Volume}} = \frac{\left(\frac{3}{2}\right)+3+\left(\frac{3}{2}\right)}{\frac{3\sqrt{3}}{2}a^2c} = \frac{6}{\frac{3\sqrt{3}}{2}(d^2)(2d\sqrt{\frac{2}{3}})} = 3.29846 * 10^{28}\,\frac{\text{ions}}{\text{m}^3} \tag{S4}$$

Thus, the total of all ion concentrations at the closest approach to the interface must be approximately equal to or less than this atomic density.

$$n_{\,max} \leq 3.29846 * 10^{28}\,\frac{\text{ions}}{\text{m}^3} \tag{S5}$$

Summing up the concentration of all hydrated ions in solution at the interface means summing up the value from Equation S3 for each hydrated ion:

$$\sum n_i = \sum n_i^0 e^{\left(\frac{-z_i e \phi (V3-V4)}{kT}\right)} \tag{S6}$$

Table C1: Concentration of solution species as a function of BTO thickness and polarity

Potential Applied to TiO_2 vs RHE	**Thickness of BTO (X_1-X_0)**	**Polarization of BTO**	**Potential Drop (V) in Solution (V4-V3)**	**$\sum n_i$ at Solution Interface ($\frac{\text{ions}}{\text{m}^3}$)**
0.4V	0	None	-0.0111	1.3205×10^{27}
0.4V	5nm	Positive	-0.0105	1.3094×10^{27}
0.4V	5nm	Negative	-0.0117	1.3345×10^{27}
0.4V	40nm	Positive	-0.0034	1.2154×10^{27}
0.4V	40nm	Negative	-0.0131	1.3684×10^{27}

Material Properties Used in our Model:

Potential of bulk TiO_2 vs RHE after potential is applied:
((-4.44) + (0.59)*(pH)) + 0.135 - (potential applied vs RHE)
Where : ((-4.44) + (0.59)*(pH)) accounts for RHE potential shift as a function of pH, 0.135 accounts for the voltage difference between the Fermi level of the TiO2 we produced in our experiment and those recorded elsewhere from literature[2, 3] and 'potential applied vs RHE' is the potential recorded by the potentiostat has having been applied vs RHE (usually chosen as 0.4 for the sake of comparing calculations to

experimental data).

Potential of bulk TiO_2 vs RHE before potential is applied:

(Fermi level of TiO2 with isoelectric surface) +(0.059)*(pH - (pH of Isoelectric point of solution interface))

Where Fermi level of TiO_2 with isoelectric surface is the V vs RHE of the bulk of TiO_2 when it's surface is isoelectric: ((-4.44 - .2444) + (Flat band of TiO_2 at pH vs SCE) + (0.059)*(pH of Isoelectric point of TiO_2)).

Where 'Flat band of TiO_2 at pH vs SCE' is 0.18V[2, 3] and 'pH of Isoelectric point of TiO2' is 5.2[4] for rutile TiO_2.

The 'Isoelectric point of solution interface' is 5.2 in the case of a TiO_2/Solution interface and 5.0[5] in the case of a TiO_2/BTO/Solution interface.

pH:

Experimental value: 14

Insulator Thickness:

Measured from experiment (Fig S1) 0, 5nm, 40nm.

Temperature:

295.15K

Relative Electrical Permitivity of TiO_2:

160[3]

Relative Electrical Permitivity of BTO:

1500[6]

Relative Electrical Permitivity of H_2O:

80

Bandgap of Rutile TiO_2:

3.02eV[7]

Donor Concentration in TiO_2:

$9 * 10\text{^}18$ / cm^3[8]

Bulk Concentration of Electrons in TiO_2:

Donor Concentration in TiO_2

Concentration of Holes in TiO_2:

Mass action with intrinsic electrons

Density of States in the Conduction band of TiO_2:

$1 * 10\text{^}20$ / cm^3[9]

Remnant Polarization of BTO:

Measured from experiment (Figure S5): $5 * 10\text{^} - 6$ uC/(cm^2)

Supplemental figures

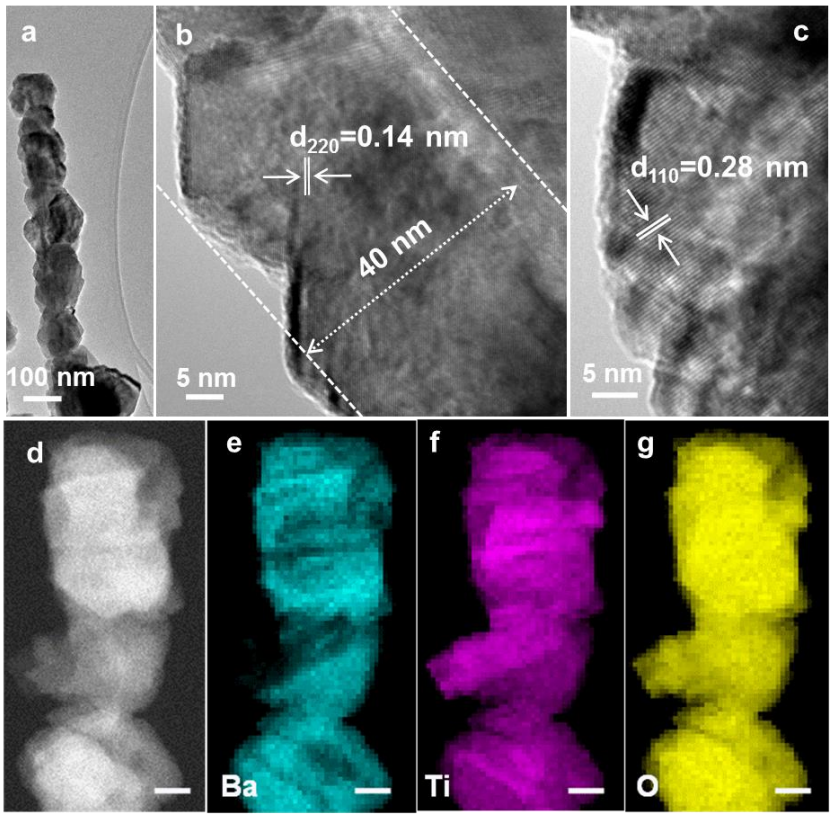

Figure S1. Structure and elemental characterizations of 210 °C TiO_2/BTO core/shell NWs. **(a)** Representative TEM image and **(b, c)** high-resolution TEM images of a 210 °C TiO_2/BTO core/shell NWs. The BTO shell thickness was measured to be ~40nm. A lattice spacing of 0.28 nm in the shell corresponds to the (110) plane of tetragonal BTO. **(d)** STEM image of a 210 °C TiO_2/BTO core/shell NW. **(e-g)** EELS elemental mapping images for Ba (e), Ti (f) and O (g), respectively. Scale bars are 20 nm.

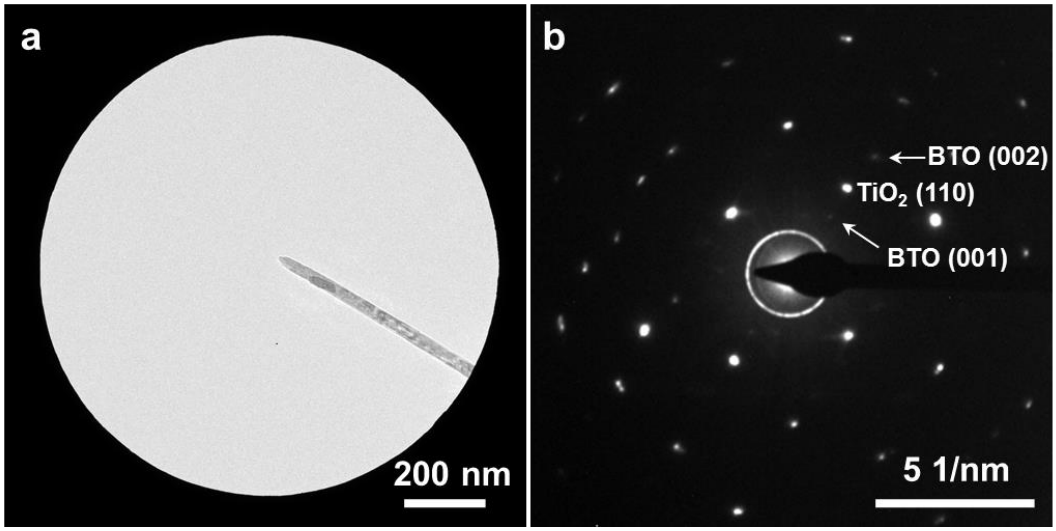

Figure S2. (a) TEM image of an individual 150 °C TiO_2/BTO core/shell NW. (b) Corresponding selected area electron diffraction (SAED) pattern, showing the perpendicular c-axis of TiO_2 and BTO.

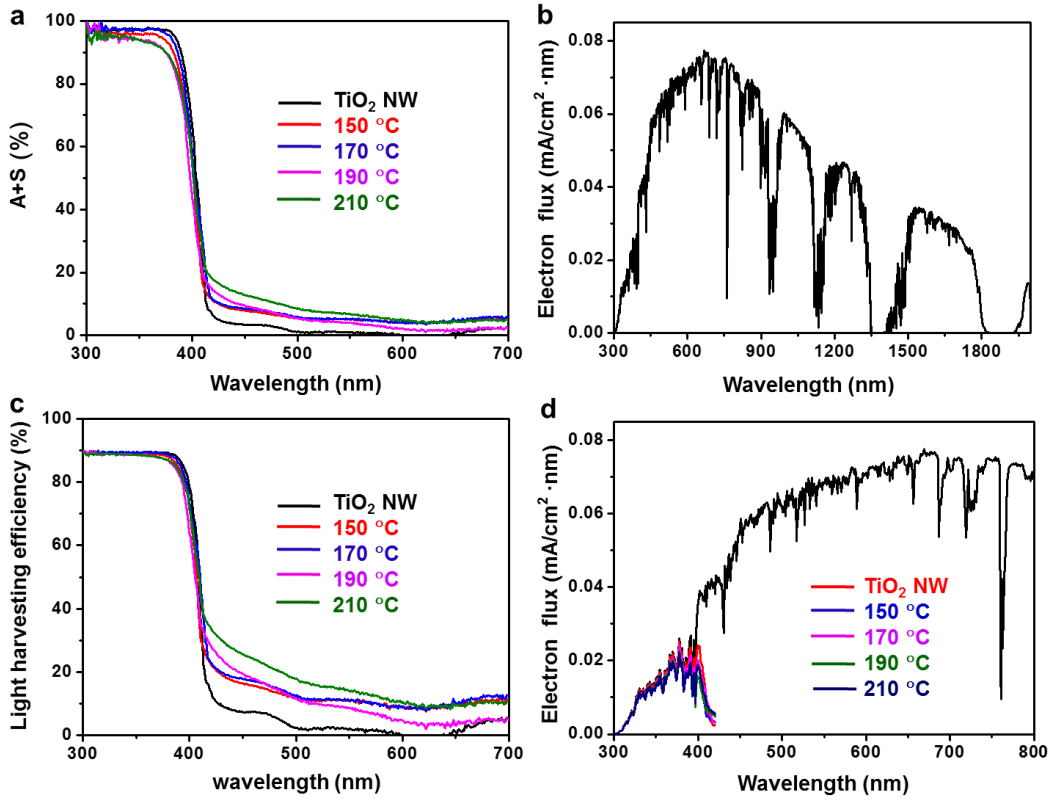

Figure S3. (a) UV-visible absorption of TiO_2 NWs and TiO_2/BTO core/shell NWs with different conversion temperatures (150-210 °C). Absorption (A) + scattering (S) = 100 – transmittance (T) – reflectance (R). The integrated light absorption (plus scattering) values over 300-420 nm were 84.5%, 81.9%, 84.6%, 80.0% and 81.7% for the TiO_2 NWs and TiO_2/BTO core/shell NWs with the conversion temperature of 150-210 °C, respectively. **(b)** Electron flux of AM 1.5G solar spectrum. **(c)** The light harvesting efficiencies (η_{LHE}) of TiO_2 NWs and TiO_2/BTO NWs with different conversion temperatures (150-210 °C). η_{LHE} was calculated from the absorbance data (η_{ABS}) shown in Figure S2a: $\eta_{LHE} = (1\text{-}10^{-\eta ABS}) \times 100\%$. **(d)** Electron flux of the TiO_2 NWs and four TiO_2/BTO NWs photoanodes. The electron flux of photoanode was the product of the AM 1.5G electron flux and η_{LHE}. Photocurrent density (J_{abs}) under 100% absorbed photon conversion efficiency can be estimated by integrating the electron flux at the photoanodes across 300-420 nm wavelength range.

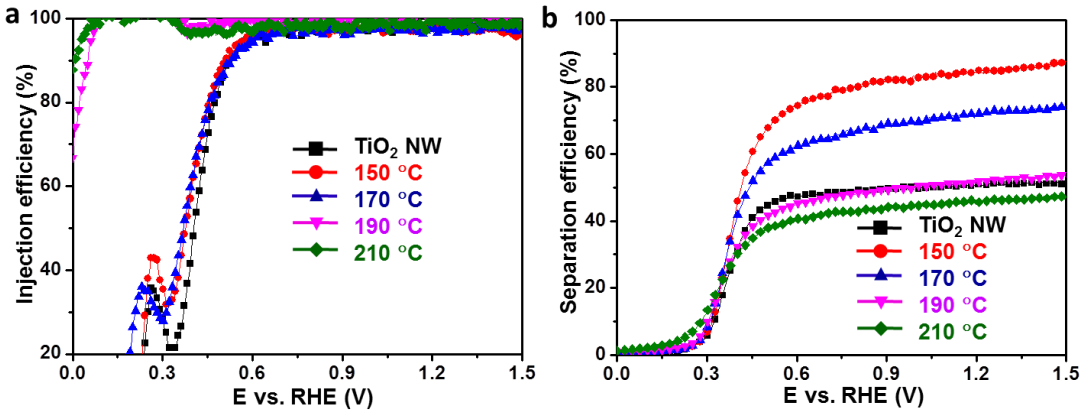

Figure S4. (a) Efficiency of charge injection from the photoanodes to the electrolyte within the full bias window. **(b)** Efficiency of charge separation inside the photoanodes within the full bias window.

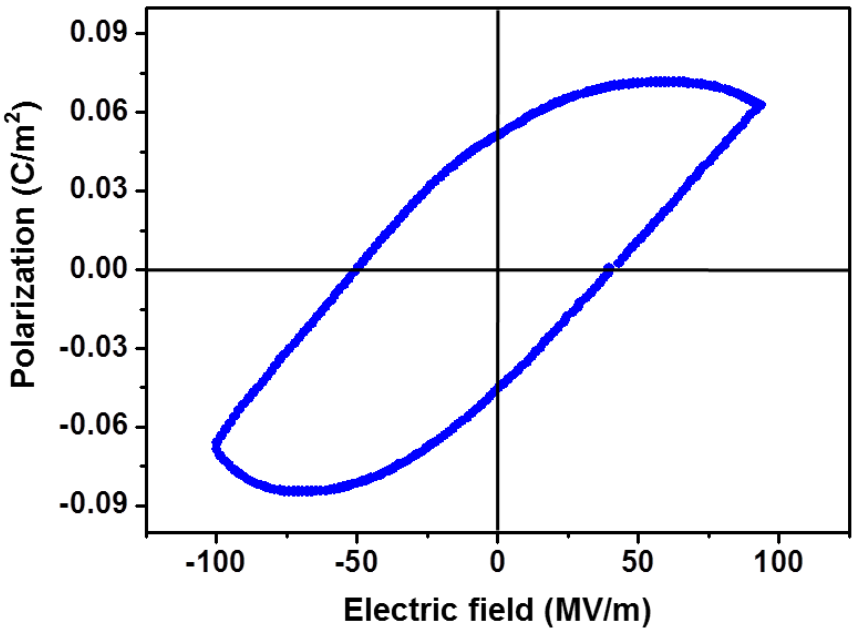

Figure S5. Polarization-electric field hysteresis loop measured on the 150 °C TiO_2/BTO NWs at room temperature.

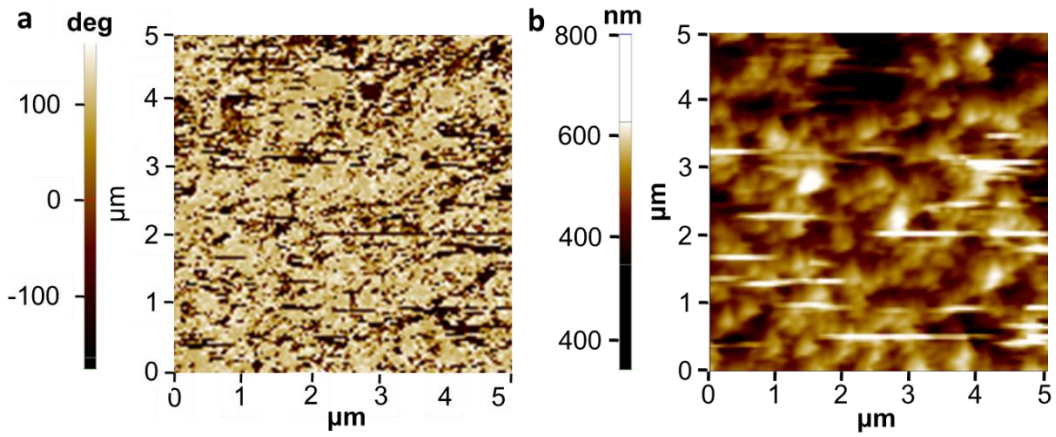

Figure S6. (a) DC-EFM phase images of the TiO_2/BTO core/shell NWs with the conversion temperatures of 150 °C, representing its spontaneous polarization direction. **(b)** DC-EFM topography images of the TiO_2/BTO core/shell NWs with the conversion temperatures of 150 °C.

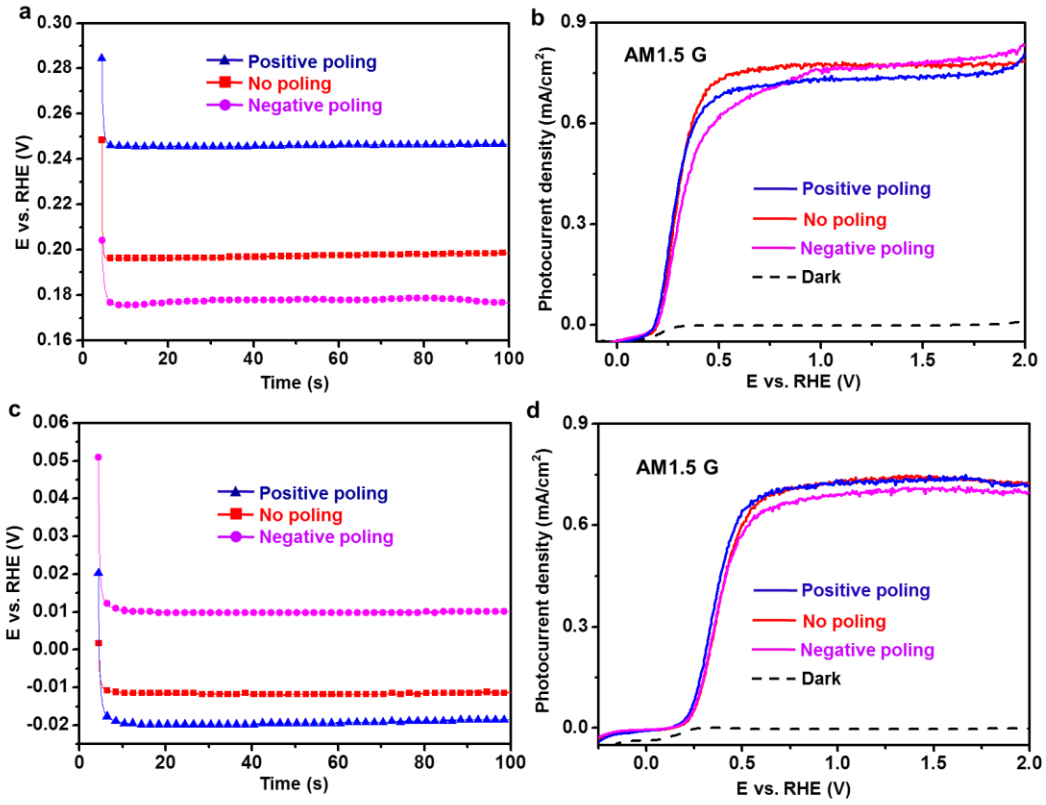

Figure S7. (a) Chronopotentiometric curves of the as-prepared (red), positively poled (blue) and negatively poled (magenta) 150 °C TiO_2/BTO NWs measured in 1 M NaOH electrolyte under AM1.5 G illumination with a constant current of zero, demonstrating their onset potentials were 197, 246 and 178 mV, respectively. **(b)** *J-V* curves of the as-prepared (red), positively poled (blue) and negatively poled (magenta) TiO_2 NWs under one sun illumination. TiO_2 NWs were poled under 3 and -2 V by solution method. **(c)** Chronopotentiometric curves of the as-prepared (red), positively

poled (blue) and negatively poled (magenta) 210 °C TiO_2/BTO NWs measured in 1 M NaOH electrolyte under AM1.5 G illumination with a constant current of zero, demonstrating their onset potentials were -12, -19 and 10 mV, respectively. **(d)** *J-V* curves of the as-prepared (red), positively poled (blue) and negatively poled (magenta) TiO_2 NWs under one sun illumination. TiO_2 NWs were poled under ±100 V in air.

Reference

1. Liu, B.; Aydil, E. S. *J. Am. Chem. Soc.* **2009,** *131*, 3985-3990.
2. Hu, K.; Fan, F.-R. F.; Bard, A. J.; Hillier, A. C. *J. Phys. Chem. B* **1997,** *101*, 8298-8303.
3. Kavan, L.; Grätzel, M.; Gilbert, S. E.; Klemenz, C.; Scheel, H. J. *J. Am. Chem. Soc.* **1996,** *118*, 6716-6723.
4. Bullard, J. W.; Cima, M. J. *Langmuir* **2006,** *22*, 10264-10271.
5. Blanco López, M. C.; Rand, B.; Riley, F. L. *J. Eur. Ceram. Soc.* **2000,** *20*, 107-118.
6. Kennedy, J. H. *J. Electrochem. Soc.* **1976,** *123*, 1683.
7. Scanlon, D. O.; Dunnill, C. W.; Buckeridge, J.; Shevlin, S. A.; Logsdail, A. J.; Woodley, S. M.; Catlow, C. R.; Powell, M. J.; Palgrave, R. G.; Parkin, I. P.; Watson, G. W.; Keal, T. W.; Sherwood, P.; Walsh, A.; Sokol, A. A. *Nat. Mater.* **2013,** *12*, 798-801.
8. Lim, H.; Jang, H. W.; Lee, D. K.; Kim, I.; Hwang, C. S.; Jeong, D. S. *Nanoscale* **2013,** *5*, 6363-6371.
9. Nagao, Y.; Yoshikawa, A.; Koumoto, K.; Kato, T.; Ikuhara, Y.; Ohta, H. *Appl. Phys. Lett.* **2010,** *97*, 172112.